Molecular and cellular processes of deafferentation after plexus injury in human dorsal root ganglia

Heike Rittner

Rittner_H@ukw.de

University Hospital of Würzburg

Annemarie Sodmann

University Hospital of Würzburg

Johannes Degenbeck

University Hospital of Würzburg

Annemarie Aue

University Hospital of Würzburg

Magnus Schindehütte

University Hospital of Würzburg

Felicitas Schlott

University Hospital of Würzburg

Panagiota Arampatzi

University of Würzburg

Thorsten Bischler

University of Würzburg

Max Schneider

University of Ulm

Camelia Monoranu

University of Würzburg

Tom Gräfenhan

University of Würzburg   https://orcid.org/0000-0002-3653-4851

Michael Bohnert

University of Würzburg

Mirko Pham

University Hospital of Würzburg

Gregor Antoniadis

Ulm University, District Hospital Günzburg

Robert Blum

University Hospital of Würzburg

Article

Additional Declarations: (Not answered)

Abstract

Plexus injury results in lifelong suffering from flaccid paralysis, sensory loss, and intractable pain. For this clinical problem, regenerative medicine concepts set high expectations. However, it is completely unknown how dorsal root ganglia (DRG) are affected by accidental deafferentation. Here, we investigated human DRG in a clinically characterized cohort of patients with plexus injury. Avulsed DRG from 13 patients were collected during reconstructive nerve surgery. DRG were analyzed using large-scale microscopy, deep learning-based bioimage analysis, and RNA fragment sequencing of histopathological slices. In about half of the patients, we found a complete loss of DRG units consisting of neurons, satellite glial cells (SGC), and macrophages. The DRG cells were replaced by mesodermal/connective tissue. In the other half of the patients, the cellular units were well preserved and we found no gliosis and no significant neuronal loss. Furthermore, the expression of subtype-specific sensory neuron marker genes was preserved. However, downregulation of neuronal attributes associated with ion transport, synapses, and neuronal projection indicated a dormant neuronal phenotype. Injured DRG showed signs of ongoing inflammation and connective tissue remodeling. Patients with 'neuronal preservation' had less pain than patients with 'neuronal loss'. Arm function improved after the nerve reconstruction, but the pain phenotype did not. With this study, we call for early intervention after injury to protect the DRG from complete cell loss. Pain patients may benefit from anti-inflammatory therapy. Future regenerative medicine concepts will need at least two translational directions: reafferentation of existing DRG units or replacement of the entire DRG.

INTRODUCTION

Brachial plexus injury mainly occurs after traffic accidents and is associated with profound functional impairments. Typically, during the accident, ventral and dorsal roots are avulsed at the dorsal root entry zone. In upper supraclavicular brachial plexus injury, 69–84% of patients with total palsy report pain (1, 2). This often results in lifelong disability of patients in the middle of their life (3). Surgical interventions include neurolysis, nerve grafting, nerve transfer, and muscle or tendon transfer to restore motor function (4, 5). However, sensory function and pain are barely improved by the surgery: mean pain decreases only by 1.2 points on the numerical analog scale (NRS) (3). In fact, patient consider ΔNRS from 2 as clinically relevant (6). Several mechanisms can explain increased pain after nerve injury: lack of sensory input, ectopic firing in the dorsal horn, increased activity of regenerating axons and collaterals, maladaptive peripheral nociceptor input, as well as central sensitization (7).

To restore sensory functions, repair of different motor-, sensory and nociceptive structures of the nervous system could be helpful (8). Thus, neural replacement strategies set high expectations (9). However, up to date, the cellular changes after plexus injury in humans are not known. Without this knowledge, it is virtually impossible to design new treatments including regenerative medicine, cell-targeted immunotherapy, or pathfinding strategies (10, 11).

Very few studies have analyzed plexus injury; so, most evidence has firstly been extrapolated from more peripheral nerve lesions and secondly almost exclusively from rodents. These injuries lead to adaptions in the DRG cell composition and cellular plasticity in the whole DRG (*12–15*). Loss of sensory neurons seems to depend on the severity of injury (*15*). Satellite glial cells (SGC), a cell type that forms a functional unit with the sensory neuron soma, react within hours after nerve injury and contribute to pain by enhancing neuronal excitability (*16*). Typical plasticity responses of SGC, for instance after ventral root avulsion or spared nerve injury (*12, 17*), include an increased expression of the glial fibrillary acidic protein (GFAP) or apolipoprotein J (APOJ) (*14, 16, 18*). Furthermore, macrophages become activated, invade, or proliferate locally in the DRG close to the neuron-SGC unit (*17, 19, 20*). Recent studies used modern transcriptomics and cell profiling techniques to characterize neurons and non-neuronal cells of the human DRG (*21–26*). These studies revealed evolutionarily conserved molecular and cellular signatures in the mammalian DRG, but also showed distinct human-or disease-specific features. After nerve injury, in peripheral painful neuropathy, inflammatory genes associated with macrophages are elevated and neuronal genes are downregulated. Furthermore, histological analysis indicated different degrees of loss of ganglion neurons with replacement fibrosis (*27*). In addition, *Ray et al.* investigated DRG tissue harvested from neuropathic pain patients with thoracic vertebrectomy (*28*). Transcriptome analysis revealed different sets of candidate genes as potential drivers of neuropathic pain. Importantly, substantial sex differences, a dominant neuro-immune phenotype, and regulation of distinct cytokine signalling pathways were observed (*27*).

Here, we clinically phenotyped a cohort of patients with brachial plexus injury and asked how deafferentation of the DRG affects their molecular and cellular composition. Avulsed DRG were collected during nerve reconstruction surgery and analyzed by immunohistochemistry, large-scale tile microscopy, human DRG-adapted deep learning-based algorithms (*29*), and new concepts for quantitative assessment of the neuron-satellite-glia unit (*12*). For in depth-analysis of molecular markers, we established RNA fragment sequencing of the histopathological slices. Our data document that patients suffering from plexus injury can be categorized into two groups: patients with either total loss or patients with complete preservation of the multicellular DRG unit. In patients with neuronal preservation, transcriptome analysis indicates a 'deafferentation phenotype' with reduction of functional neuronal parameters, no signs of functional recovery, and replacement by connective tissue.

RESULTS

Patients with plexus injury: clinical data of the cohort

The plexus injury group was comprised of 13 mostly male patients – on average five months after brachial plexus injury, typically due to a motorcycle accident (Table 1). Patients suffered overall from complete avulsion of two to three dorsal roots. Usually, five segments were affected by the trauma.

Table 1
Clinical characteristics of study subjects.

Parameter	Patients with plexus injury (n = 13)
Age (years)	34.7 ± 13.8
Sex	f: 2, m: 11
Type of accident	motorcycle: 8, other: 5
Time since injury (months)	4.7 ± 1.3
Number of dorsal roots affected	
Affected by Dorsal Root Avulsion	2.8 ± 1.2
Affected by all lesions	4.6 ± 0.9
Pain	
Current pain (numeric rating scale, NRS 0−10)	4.7 ± 2.2
Mean pain (numeric rating scale, NRS 0−10)	5.0 ± 2.3
Maximum pain (numeric rating scale, NRS 0−10)	7.6 ± 1.8
Graded chronic pain scale (GCPS, I-IV)	2.8 ± 1.2
Disability and neuropathic pain	
Disability arm, shoulder, and hand (DASH): total symptom score	51.2 ± 15.4
Disability arm, shoulder, and hand (DASH): work score	80.0 ± 22.2
Neuropathic pain symptom inventory (NPSI, 0−1)	0.3 ± 0.2
Psychiatric comorbidities	
State-Trait Anxiety Inventory: State (STAI-S, 20−80)	45.5 ± 13.3

GCPS: grade I-IV; I, low disability-low intensity; II, low disability-high intensity; III, high disability-moderately limiting; IV, high disability-severely limiting. NPSI: no cut-off. STAI: STAI-S ≤ 39 defined as normal. BDI II: 0−13 minimal, 14−19 mild, 20−28 moderate, 29−63 severe depression. PCS: 0−29 low, 21−37 moderate, 38−52 high catastrophizing tendency. DASH: no cut-off. Treatment refers to medication prescribed at hospital discharge after reconstructive surgery, multiple medications possible. All data are mean ± standard deviation.

Parameter	Patients with plexus injury (n = 13)
State-Trait Anxiety Inventory: Trait (STAI-T, 20–80)	41.7 ± 15.7
Beck depression inventory 2 (BDI II, 0–63)	14.8 ± 13.9
Pain catastrophizing scale (PCS, 0–52)	22.5 ± 12.1
Treatment (number of patients)	
Non-opioid analgesics	11
Opioids	4
Anticonvulsants	9
Antidepressants	7
Cannabinoids	1
No analgesics	0
	Control group (n = 5)
Age (years)	68.0 ± 23.5
Sex	f: 2, m: 3
Cause of death	accident: 2, accident or cardiovascular disease: 1, suicide: 1, cerebral venous sinus thrombosis: 1
Interval before autopsy (IBA, days)	3.8 ± 1.3
Interval before autopsy without cooling	1 h of IBA: 2, 2 h of IBA: 2, n. a.: 1

GCPS: grade I-IV; I, low disability-low intensity; II, low disability-high intensity; III, high disability-moderately limiting; IV, high disability-severely limiting. NPSI: no cut-off. STAI: STAI-S ≤ 39 defined as normal. BDI II: 0–13 minimal, 14–19 mild, 20–28 moderate, 29–63 severe depression. PCS: 0–29 low, 21–37 moderate, 38–52 high catastrophizing tendency. DASH: no cut-off. Treatment refers to medication prescribed at hospital discharge after reconstructive surgery, multiple medications possible. All data are mean ± standard deviation.

Patients presurgically described moderate mean pain, high maximum pain, and moderate neuropathic pain quality (Neuropathic Pain Symptom Inventory) (Table 1). Half of the patients reported a higher level of state anxiety – four of these moderate to severe depressive symptoms (Table 1). Pain catastrophizing (PCS) was on average below the threshold. The DASH score revealed that all patients were highly impaired in their upper extremity activities – in daily life and even more at work.

All patients received pain medication. The most frequently prescribed drug class was non-opioid analgesics, followed by anticonvulsants and antidepressants. Four patients received opioids and one cannabinoids (Table 1). The control cohort data were acquired from five cases scheduled for forensic autopsy (Table 1). The control group was 27.8 years older than the patient cohort.

Either 'neuronal loss' or 'neuronal preservation' in patients with plexus injury

Human DRG showed fiber-rich regions interrupted by neuron-rich regions (Fig. 1). Neuron-rich areas were predominantly localized in the periphery of DRG sections. A thick, protective connective tissue layer surrounded DRG and was also found between neuronal somata. All neuronal somata contained a nucleus with a prominent nucleolus and were surrounded by SGC. Surprisingly, in seven of the 13 patient tissue samples, neither neurons nor SGC were found. To be sure that this was true for the whole putative DRG, we stained serial slices with H&E throughout the whole DRG, but could not find any neuron/SGC units. Only fat cells and connective tissue were found next to nerve fibers. In controls obtained from forensic autopsy, DRG tissue was preserved and comparable to that of plexus injury patients with neuronal preservation.

Presurgical magnetic resonance neurography did not allow reliable delineation of the affected DRG from injured adjacent neural structures in either 'neuronal loss' or 'neuronal preservation' patients. In Fig. 1H, a 'neuronal preservation' patient with an intradural avulsion of the left C8 and T1 roots is shown. Here, the retracted nerve stumps form a neuroma and did not allow delineation of the affected DRG due to post-traumatic fibrous scarring and adhesions. Figure 1J is representative of a 'neuronal loss'-patient. An intradural avulsion of the right C7 and C8 root is visible. Retracted nerve stumps formed a neuroma and we could not delineate the affected DRG. On the contralateral sides, the unaffected DRG, segments C5-C8, could be properly identified.

In the clinical examination, areas of pain and loss of sensation did not match injured segments (Fig. 2). Most patients felt pain and sensitivity alterations in dermatomes of both injured and non-injured segments. Even when all kinds of lesions – avulsions of the corresponding dorsal or ventral roots, more peripheral nerve lesions, lesions of the spinal cord or bone fractures – were considered, pain and sensitivity alterations were reported in dermatomes in- and outside of the injured segments (5 out of 13 for pain and 3 out of 13 for sensation). Trait-anxiety and catastrophizing correlated significantly with the von Korff's Graded Chronic Pain Scale (GCPS) (Fig. 2). The highest activity impairment was reported by patients with symptoms of depression and anxiety (Fig. 2). Mean pain intensity was associated with functional upper extremity impairment evaluated in the Disability of the Arm, Shoulder, and Hand score (DASH) (Fig. 2).

Patients with neuronal loss had more pain, tendentially more injury, and received more analgesics (combination of anticonvulsants and antidepressants, Fig. 2, table S1). The majority of the patients with 'neuronal loss' perceived pain as 'deep' feeling pressuring and squeezing as measured by the clusters of the NPSI (30), whereas most 'neuronal preservation' patients perceived pain as 'pinpointed', reporting

paresthesia. Of note, none of the patients was in the 'evoked pain' cluster – experiencing pain provoked by brushing, pressure, or cold.

A follow-up survey on selected clinical outcomes was conducted by interviewing the 13 plexus injury patients via telephone, 10–30 months after surgery. The comparison of outcomes at the timepoint of surgery (T0) and the time point of the telephone interview (T1) reveals post-surgical improvements in functionality, e.g. key turning and door opening (Fig. 3, **table S2**), but pain remained unchanged. Neuropathic symptoms, like squeezing pain, tingling and allodynia, even got worse. The 'neuronal loss' patients continued to have more pain than the 'neuronal preservation' patients (**table S3**).

Cellular plasticity and satellite glia cell marker distribution in human DRG

To investigate the cellular composition of the avulsed DRG, we used triple color immunofluorescence. Labels were first validated with high resolution confocal microscopy (Fig. 4). NF (*neurofilament*) and MAP2 (*microtubule-associated protein 2*) were reliable markers for neurons and labeled sensory neuron somata of all sizes (Fig. 4). Intracellular lipofuscin aggregates with substantial autofluorescence were observed in all samples. Almost all sensory neuron somata were surrounded by FABP7 (*fatty acid binding protein 7*)-positive SGC, whereas GS (*glutamine synthetase*) and GFAP (*glial acidic fibrillary protein*) signals were seen far more sparsely in both patient and control DRG (**fig. S1**). Anti-APOJ (*clusterin*) immunoreactivity also stained ring-like structures around NF-positive neuronal somata and was largely co-localized with the SGC marker FABP7. Macrophages labeled by IBA1 (*allograft inflammatory factor 1*) were present in the DRG around NF- and MAP2-positive neuronal somata. Some macrophages were also seen in the surrounding connective tissue.

Unaltered cellular composition in the 'neuronal preservation' group

In a second step, complete slices were imaged with large-scale tile microscopy (Fig. 5A,B). Tissue sections from different patients showed a high cellular heterogeneity (**fig. S1**). To objectively analyze the cellular composition (**fig. S2**), we used a recently introduced deep learning (DL)-based analysis strategy for microscopy images (*12*). First, DL models needed to be trained to allow computational segmentation of the neurons in the human DRG. For this, three experts annotated NF-positive neurons in representative human DRG images. Subsequently, a computational consensus information of all experts (ground truth) was computed and used to train DL-model ensembles. This strategy has been shown to increase the objectivity and validity of bioimage analysis (*29, 31*). Expert annotations overlapped highly with the ground truth estimation (**table S4**). DL-models, validated with different ground truth image data sets, reached a mean *dice score* of 0.875 (**table S5**), thus confirming reliable sensory neuron segmentation in the human DRG. Testing of the DL-model ensemble was performed on annotated images that were

previously not seen by the DL-model. This control test showed that the trained DL-model predicted segmentations of NF-positive neurons in the human DRG with human expert-like performance (**fig. S2**).

Neuronal somata of control DRG were slightly smaller than those of patients with 'neuronal preservation' but the neuronal density did not differ (Fig. 5). Almost all (95%) of the DRG neurons were in proximity to SGC (FABP7-positive SGC), showing that the unit of sensory neurons and their SGC was well preserved. Furthermore, similar numbers of FABP7-positive cells occupied the neuron near area, indicating the absence of gliosis. No upregulation of the injury-related factor *clusterin* (APOJ) in SGC was computed based on APOJ intensity in FABP7-positive SGC. A trend towards higher macrophage abundance close to neurons was found in patients. The data show that the multicellular composition of the DRG, consisting of sensory neurons of different sizes, their SGC ring, and neuron-near macrophages, was preserved in patients after plexus injury.

Downregulated attributes of neuronal communication in the 'neuronal preservation' group

To investigate the molecular signature of the histopathological tissue samples, we performed RNA sequencing. We were faced with three major challenges: (1.) Tissue needed histological pre-examination in order to identify tissue section with DRG units. (2.) Patient recruitment and access to the human DRG tissue was a year-long process. (3.) The degenerative state of the tissue was not fully controllable. Thus, we decided to collect PFA-fixed, pre-examined histological slices of the plexus injury patients and the corresponding controls from the forensic autopsy. As we expected to get degraded RNA from the PFA-fixed slices, we performed bulk sequencing of RNA fragments. For this, the RNA isolation procedure was optimized to ensure efficient isolation of RNA fragments longer than 200 nucleotides.

When comparing sequencing results of six samples of 'neuronal preservation' patients to six controls, we found 416 significantly up- and 394 downregulated genes (Fig. 6A, data are organized in **data file S1**). Enriched terms indicated an upregulation of extracellular matrix organization and inflammatory processes (e.g. cellular response to cytokine stimulus), whereas neuronal processes, such as synapse organization and neuron projection, were downregulated (Fig. 6B). Moreover, enriched terms were associated with the regulation of (ion) transport. We further filtered the data and computed gene ontology (GO)-terms for biological processes and cellular components (Fig. 6C). This analysis found a big gene interaction cluster for immune system processes and inflammatory responses (Fig. 6C, in red) and a distinct downregulation of neuronal attributes involved in (ion) transport, presynapse function, and neuron projection (Fig. 6C, in blue).

Upregulated genes with expression levels higher than 10 transcripts per million (TPM) encode particularly for collagen (COL1A1, COL3A1) and chemokine proteins (CCL2, CCL3, CCL4, CCL8, Fig. 6D), while downregulated genes include for example PIRT, a phosphoinositide-interacting regulator of TRPV1. In line with our previous immunofluorescence results, all immunolabeled proteins were also detected in the transcriptome. MAP2 was slightly down- and AIF1 was slightly upregulated. This supports the

pathophysiological concept with a trend towards more IBA1-positive macrophages in plexus injury patients with neuronal preservation.

We finally assessed the transcriptomic expression levels of marker genes for each patient and each control tissue (Fig. 7, **data file S2**). We specifically sorted for house keeping genes (Fig. 7A), non-neuronal cells (Fig. 7B), sensory neuron classification markers (Fig. 7C), key factors representing sensory neuron function (Fig. 7D), and marker genes used for sensory neuron subtypes found in the mouse (Fig. 7E) or human DRG (Fig. 7F). For candidate gene selection, we refer to previous studies and data sets on the molecular classification of DRG cells (*14, 19, 24, 32, 33*). Albeit the expression levels of individual genes, including house keeping genes, were quite variable between samples, the data show a broad representation of virtually all sensory neuron markers in DRG of patients with neuronal preservation. This is in accordance with the data on the cellular composition of the DRG (see Fig. 5). In the patient group, especially marker genes of macrophages and connective tissue were significantly upregulated, whereas some neuronal genes were mainly downregulated, though rarely those associated with different neuronal subtypes. For example, several voltage-gated potassium channels were downregulated (**Data File S2, gene list: sensory neuron genes**), but we also found upregulation of purinergic receptors.

As expected, transcriptome analysis of slices from two neuronal loss patients and one excluded control sample confirmed the absence of expression of sensory neuron marker genes, the difference to the other samples, and the need to exclude these (**Fig. S3**).

DISCUSSION

In our study, we examined the effects of deafferentation on the human DRG at the time of plexus reconstruction, in a cohort of patients with plexus avulsion. Surprisingly, patients fell into two dichotomous groups: plexus injury patients with 'neuronal preservation' or with 'neuronal loss'. Contrary to our hypothesis, in DRG with 'neuronal preservation', we observed neither less neurons, nor an upregulation of GFAP in SGC, nor gliosis. However, we found increased inflammatory responses and extracellular matrix organization, and downregulation of functional neuronal processes associated with presynaptic function, (ion) transport, or neuronal projection. So, this injury at the boundary between the PNS and the CNS seems to evoke (1.) an 'all-or-none' response and (2.) a neuronal dormant state in remaining DRG in a biological context of increased inflammation and ongoing tissue remodeling.

The clinical presentation of our cohort was representative (*34–36*): all patients had pain with some neuropathic symptoms and were largely impaired in daily life (*1, 3*). Among the typical disease burden coming from flaccid paralysis, numbness, and intractable pain, a quarter of our patients reported symptoms of depression and increased anxiety levels – as shown in other cohorts (*37*). Pain had squeezing and pressure quality comparable with 'deep pain' in the NPSI clusters (*30*) and was not restricted to the corresponding dermatomes of the injured segments. This could be due to collateral damage, root overstretching, or plastic changes due to aberrant innervation from collateral or regenerating nerves. Spontaneous or ectopic activity from these damaged neurons can cause

spontaneous or shooting pain (*38*). Input from nociceptors is necessary because the application of local anesthetics to adjacent roots relieves pain (*39*). Disruption of the pain pathway might also spread to other ipsilateral DRG or may lead to central sensitization and/or ectopic activity originating in the dorsal horn. We do not know the reason why half of the patients lost their DRG tissue, but these patients had a tendency towards more widespread injury. Thus, it is possible that more injury resulted in hematoma formation, disruption of blood supply, more inflammation and scarring, mitochondrial collapse, and anoxic death. Pain is the major limitation for return to work and quality of life after plexus injury. Most of our patients received anticonvulsants and non-opioids, although, for neuropathic pain, antidepressants have a better efficacy (*40*). Even after a nerve reconstruction surgery, neuropathic pain persisted, despite improved functionality. Conceptually, a treatment aiming at the restoration of sensory and nociceptive pathways might help here – interestingly, neonates with plexus injury have an excellent sensory recovery and rarely develop pain (*41*). This argues that an intact somatosensory system is necessary for pain relief (*41*), thus making neural replacement strategies conceptually attractive.

In preclinical models, the 'neuronal loss' phenotype has, to our knowledge, never been observed. SGC are activated in response to peripheral postganglionic and preganglionic injury, as well as dorsal or ventral root avulsion (*17, 42, 43*). In human tissue, we did not detect any signs of gliosis using typical SGC markers like GS, and FABP7. GS showed only a low expression in our human DRG. In line, others found it in 10% of human SGC on mRNA and protein level (*24*) – so it does not seem to be a good marker in humans. Across species, 88–96% of neurons are surrounded by FABP7-positive SGC. This is in line with our data showing 95% SGC-neuron units (neurons in proximity to FABP7-positive SGC) in both groups. For SGC activation (*18*), we saw very low GFAP abundance and high APOJ expression in all samples, independent of injury. This is also supported by the transcriptome data and data by others (*24*). Additionally, we found, in line with others, local macrophages close to the neuron/SGC unit (*44*). Thus, the cellular DRG unit with neurons, SGC, and local macrophages is preserved in some patients, whereas it completely disappears in others.

Interestingly, even though neurons were preserved in some patients, we found a reduction in genes associated with neuronal processes and compartments, such as neuronal projection (e.g. PRPH), synapses (e.g. NTRK1), and ion transport (e.g. TRPV1). This could indicate that the deafferentation itself does not induce neuronal loss, only loss of neuronal function. Moreover, inflammatory processes and extracellular matrix organization were increased. Inflammation and downregulation of neuronal genes were also seen in painful diabetic neuropathy (*27*), although the study reports a loss of human sensory neurons. Given the variability of the data, we cannot argue for sensory neuron death in our patient cohort with 'neuronal preservation' when compared to the control samples. In both groups, we find DRG with neuron-SGC units and a broad expression of sensory neuron subtype markers, indicating that deafferentation is not upstream of ultimate signaling events leading to sensory neuron death. So, deafferentation and peripheral nerve damage might affect sensory neurons very differently; one leading to loss of sensory functions, while the other might promote neuron death and subsequent replacement with connective tissue. Possible explanations include factors of time (long-lasting diabetes vs. 5 M

avulsion), metabolic toxicity, or the preserved connection to the spinal cord and therefore disease-specific activity events in diabetes.

Our study has several limitations. In our á priori planning, we did not expect to find patients with a complete loss of DRG neurons. It is important to note that we are sure that we isolated the representative 'DRG' tissue in case of the neuronal loss group. The two patient groups are rather small, hence, the clinical data have low statistical power. This could not be avoided, due to a rare disease and limitations in the ethical approval, because DRG after plexus injury are typically not removed during nerve reconstruction. Our patient sample was therefore restricted to a small number of patients to allow hypothesis-generating research. Secondly, DRG after plexus injury were compared with post-mortal DRG (3–6 d after death). These control samples were not easy to match with the experimental DRG samples. Moreover, human DRG tissue contains a substantial amount of connective tissue and is quite variable, making it difficult to keep the image exposure time constant across individual sections. To counteract this, we have adapted an – at least on the image level – objective analysis procedure, which is based on feature extraction in ambiguous bioimage data (*12, 45*). Human DRG tissue samples are so valuable that the bioimage data, the deep learning models, the annotated images, and the transcriptome data are helpful research tools in our open science community. They can be shared and reused, thus supporting research on human DRG on the way to new therapies.

In summary, the DRG seems to have several options for responding to nerve injury, depending on the location of the lesion, the noxe and the extent of the injury. Future MRI methods should allow improved quantification of the DRG's cell body-rich area to stratify the neuronal status non-invasively, at best over the course of the disease, to better understand when and why neuron/SGC units are lost (*46*). Restoration of the somatosensory system could resolve pain in the future. Different strategies will be necessary for 'neuronal loss' and 'neuronal preservation' patients.

MATERIALS AND METHODS

Patient recruitment

The study was approved by the local ethical committee (plexus injury patients: 32/19, cases from forensic autopsies: 205/20) and registered at the Germany clinical trials registry (DRKS00017266). The cohort was comprised of 13 patients of both sexes after brachial plexus injury, most often due to a motorcycle accident. All patients endured multiple injuries, including avulsion of the dorsal and ventral root. Study participants gave written informed consent. For a 17-year-old patient, a parent gave consent. Three to eight months after the accident, avulsed cervical DRG were collected during reconstructive surgery. The avulsed dorsal root and the corresponding DRG tissue were located, dissected, and immediately processed.

Human control DRG were obtained from seven study subjects, 3–6 days post-mortem, during routine forensic autopsy with potential injury of the central nervous system (Institute of Forensic Medicine,

University of Würzburg, Germany). One of the seven cases had to be excluded from the image analysis due to post-mortem tissue degradation. In another sample, the conglomerate of neurons in the extracted tissue was too small for systematic analysis.

Clinical characterization and patient reported outcomes

Preoperatively, patients underwent an MRI of the plexus and answered questionnaires on patient-reported outcomes. Additionally, clinical information on age, gender, laboratory results, and patient history, including a chart review, was obtained. The following patient-reported outcomes were used in the respective German versions (*47*): (1.) The graded chronic pain scale (GCPS, Von Korff Score, grade 0-IV) and scores for pain intensity (numeric rating scale, NRS) (*48*). (2.) The disabilities of arm, shoulder, and hand were assessed by the DASH questionnaire (*49*). (3.) Neuropathic pain characteristics were reported using the neuropathic pain symptom inventory (NPSI, range: 0–1) (*30*). Patients were also requested to draw the localization of their pain. (4.) Depression was assessed using the Beck Depression Inventory II (BDI II, range: 0–63). A value of 0–13 was characterized as minimal, 14–19 as mild, 20–28 as medium, and 29–63 as severe depression (*50*). (5.) The State-Trait Anxiety Inventory (STAI-T, STAI-S, range 20–80) examined anxiety as a state or trait characteristic (*51*). (6.) The pain catastrophizing scale (PCS) was used with 0 being the lowest and 52 the highest pain catastrophizing (*52*). For telephone interviews, a question sheet with selected items was created and used in a follow-up survey, 10–30 months after surgery. The question sheet was based on the Ulm questionnaire, a plexus-specific outcome questionnaire (*53*).

Magnetic resonance neurography of patients after plexus injury before surgery

Patients were examined at the Department of Neuroradiology of the University Hospital Würzburg, between 06/2020 and 03/2022. MR neurography examinations were carried out on a 3 Tesla unit (MAGNETOM Skyra, Siemens Healthineers). The same examination protocol was applied to all patients and was specifically developed for post-traumatic imaging of the brachial plexus from the spinal nerve root level to the distal levels in the axilla. Part of the extensive clinical protocol was the SPACE (3D turbo spin echo with variable flip angle) STIR (short tau inversion recovery) sequence with TR/TE 2500/208 ms, TI 210 ms, parallel imaging (GRAPPA 3, reference lines PE 24), slice thickness 1.0 mm, number of slices 104, FOV 305 x 305 mm^2, acquisition matrix 305 x 305, pixel spacing 0.95 x 0.95 mm^2 and an acquisition time of 6:19 min. The sequence was acquired using a custom-designed coil dedicated to high-resolution imaging of the supra-, retro- and infra-clavicular brachial plexus (Variety 16-Channel Multipurpose Coil, NORAS MRI product). This two-element 2 x 8-channel surface coil was positioned on the corresponding body surface on the affected side. Multi-planar image reconstruction was performed with isotropic voxel size.

Assessment of the extent of brachial plexus injury

On a first level of analysis, we counted all dorsal root avulsions, regardless of whether they were stated as complete, partial, or suspected in the presurgical MRI and doctor's reports. In a second analysis, we added

the number of segments that were affected by any kind of lesion, e.g. peripheral nerve or spinal cord injuries, or bone fractures. Areas of pain or sensitivity alterations were obtained from the patients' and doctors' reports and assigned to corresponding dermatomes. Sensitivity changes included hyperalgesia, allodynia, dysesthesia, a positive Tinel's sign, hypoesthesia, or a complete loss of sensitivity.

Tissue preparation

Immediately after tissue harvest, human DRG were transferred into ice-cold 4% paraformaldehyde/PBS solution. DRG were transported on ice and were fixed overnight at 4°C. The next day, the tissue was washed three times for 30 min in phosphate-buffered saline (PBS) and stored overnight in 30% sucrose (PBS-buffered) for cryoprotection (4°C). Afterwards, the DRG was cut longitudinally into two pieces. Each half was embedded in O.C.T. compound (Tissue-Tek) in a plastic embedding mold. Freezing was performed in 2-Methylbutane, pre-chilled with liquid nitrogen. The tissue was stored in a -80°C freezer. DRG were serially sectioned at 20 μm and mounted on twelve SuperFrost Plus slides (Menzel). Each slide contained a representative collection of 3–4 slices from different areas of the corresponding DRG. After sectioning, the slides were promptly used for immunofluorescence staining.

Hematoxylin and eosin staining (H&E)

Frozen sections were swayed for a short period of time in a 4% formaldehyde solution and afterwards in water. Then, the slides were put for 1–2 min into Mayer's hematoxylin solution. After washing in water, the slides were swayed shortly in a 1% eosin solution and were again washed in water. Then, the slides were swayed first in ethanol and afterward in xylol. Labeled sections were finally embedded in a xylene-based mounting medium (Pertex).

Immunofluorescence

Slides were incubated for 15 min in quenching solution (7.5 g/l glycine in aqua dest., pH 7.4). Labelling was performed with standard methods. In brief: blocking solution was 10% donkey or horse serum, 0.3% Triton X100, 0.1% Tween 20 in PBS. Primary and secondary antibodies were used in blocking solution (**table S6**). Cell nuclei were stained with DAPI (0.1 mg/l in PBS; 7 min). Slides were washed in PBS, shortly desalted in water, and finally embedded in Aqua Polymount (Polysciences).

Microscopy and quantitative image analysis

Tile scan microscopy was performed with an Axio Imager 2 microscope (Zeiss), a Plan Apochromat 20× (N.A. 0.8) objective, and an Axiocam 506 camera (monochromatic, 14-bit). Pixel resolution was 0.454 μm. Objective bioimage analysis was performed using *deepflash2 (45)* as described recently (*12, 29*) (*12, 29*), with some modifications. Image feature annotation was performed on 10 exemplary sections marked by neurofilament (NF) by three experts using the QuPath software (*54*). The ground truth of the annotations of the three experts was estimated with the simultaneous truth and performance level estimation (STAPLE) method (**table S4**). The *deepflash2* software created a deep learning model from these annotations (*45*). Training of a new DL-model ensemble (three models) was performed with eight of the ten exemplary images (**table S5**). Two images were used to test the model. Annotation overlap and the

model's performance were evaluated with the Dice score, defined as: $M_{Dice}(A,B) := \frac{2|A \cap B|}{|A|+|B|}$ (1); where A and B are two sets of pixels. Then, the model ensemble was applied to predict the NF-positive neurons for all images.

IBA1-positive macrophages with thin cell extensions were challenging for manual annotations. However, due to the high quality of the labels with a high signal-to-noise ratio, masks could be created with a thresholding method. First, NF-positive segmented regions were excluded from the IBA1 images to remove falsely/lipofuscin-stained parts. Then, scikit-image filters were used for background reduction and sharpening (unsharp_mask function). Calculation of an "optimal" threshold was computed with the Otsu method. Pixels with fluorescence intensity above the Otsu Threshold were considered IBA1-positive. Similarly, but without excluding neuronal regions, the masks for FABP7-positive SGC were created. Thresholding was sufficient because FABP7 almost exclusively stained SGC with a high signal-to-noise ratio. Even though the filters accounted for a lot of the variability, the DRG images of one control needed to be excluded from the subsequent analysis because the thresholding method did not work adequately for images with a low signal-to-noise ratio.

Finally, the predicted areas of neurons, SGC, and macrophages were used for image feature quantification. For this, python scripts were created https://github.com/AmSchulte/DRGhuman. The neuron-near area (NNA) was calculated through binary dilation (scikit-image morphology) of the NF segmentation. As another reference area, a convex hull was drawn to define the neuron polygon area (NPA). For SGC quantification, the area, and the proximity to neurons (percentage of neurons in proximity to FABP7-positive SGC) were used. Both the NF mask and the SGC mask were dilated by one pixel. If the overlap between a dilated neuron and the surrounding FABP7 mask was bigger than 0, the neuron was counted to be in proximity to a FABP7-positive SGC. The IBA1 area was quantified inside the NNA and the intensity of the APOJ signal was determined within the FABP7-positive SGC normalized to the rest of the APOJ intensity in the NNA. Calculated image parameters were averaged for each DRG.

RNA isolation from histopathological tissue slices

During tissue sectioning (see above) three slices, representing different regions of the DRG, we collected in 2 ml reaction tubes. Tissue was stored at -80°C until use. Patient recruitment and tissue collection took several years; hence, the PFA-fixed tissue was stored for up to 4 years. For RNA isolation, the Arcturus ™ PicoPure ™ RNA Isolation Kit (Thermo Fisher) was used. Two sets of DRG slices were combined and immersed in 200 μl of extraction buffer and 5 mM glycine was added for formaldehyde quenching. Cell lysis was performed using a bead mill (Retsch MM400) with one zirconium oxide grinding ball (5 mm) at 30 Hz for 4 min at room temperature. For higher RNA yield after fixation, the cell lysate was incubated at 65°C for 30 min in a ThermoMixer C (Eppendorf). RNA Isolation was performed according to the manufacturer's instructions. RNA columns were washed two times. The columns were dried at max. speed for three min. Samples were eluted in 15 μl elution buffer. RNA concentration was measured with a NanoDrop OneC (Thermo Fisher) and stored at -20°C until further use.

Library preparation and Sequencing

The concentration and the level of degradation (DV200) of the RNA were assessed using a Bioanalyzer (Agilent RNA 6000 Nano/Pico Kit, Agilent Technologies). Samples with DV200 > 50% were selected for further analysis. For cDNA preparation, the SMARTer® Stranded Total RNA-Seq Kit v3 - Pico Input Mammalian (Takara) with UMIs was used with 10 ng of input DNase-treated RNA. The PCR protocol was optimized by using 10 PCR cycles. The quality of the dual-indexed libraries was checked using Bioanalyzer (Agilent HS DNA kit, Agilent Technologies) and the average size was calculated at appx. 370 bp. The libraries were pooled at equimolar ratios and spiked with 5% PhiX control library. Sequencing was performed at 25 million reads/sample in paired-end mode with 54 and 68 nt read length for R1 and R2 reads, respectively, on the NextSeq 2000 platform (Illumina) using a P2 (100 cycles) sequencing kit. Demultiplexed FASTQ files were generated with BCL Convert v4.0.3 (Illumina).

Transcriptome analysis

Unique molecular identifier (UMI) sequences were extracted from the beginning of R2 reads using UMI-tools (*55*) version 1.1.1 (parameters: extract --extract-method = regex --bc-pattern2=^(?P < umi_1>.{8})(?P < discard_1>.{6}).* for all read pairs). The resulting read pairs were quality- and adapter-trimmed via Cutadapt (*56*) version 2.5 in paired-end mode (parameters: --nextseq-trim = 20 -m 1 -a NNNNNNNNNNNNNNAGATCGGAAGAGCACACGTCTGAACTCCAGTCAC ;min_overlap = 17 -A AGATCGGAAGAGCGTCGTGTAGGGAAAGAGTGT). Processed read pairs were aligned to the human genome (GRCh38.p14 primary assembly and mitochondrion) using STAR (*57*) version 2.7.2b with default parameters and junctions based on RefSeq annotation version RS_2023_03 for GRCh38.p14. Afterwards, aligned read pairs were deduplicated with UMI-tools (*55*) version 1.1.1 (parameters: dedup --paired --random-seed 123456789 --multimapping-detection-method = NH). The resulting alignment files were subsequently used for gene expression quantification via featureCounts v1.6.4 from the Subread package (*58*). Only fragments with both ends aligned to the same chromosome and strand were quantified on exon level and summarized to a fragment count for each gene. For this, multi-mapping and multi-overlapping fragments were counted strand-specific and reversely stranded with a fractional count for each aligned fragment and overlapping feature (parameters:-p -B -C -s 2 -t exon -M -O --fraction). The count output was utilized to identify differentially expressed genes using DESeq2 (*59*) version 1.24.0. Read counts were normalized by DESeq2 and fold-change shrinkage was applied by setting the parameter "betaPrior = TRUE". Differential expression of genes was assumed at an adjusted p-value (padj) after Benjamini-Hochberg correction < 0.05 and |log2FoldChange| ≥ 1.

As our libraries were constructed from total RNA, we only used protein-coding genes for further analysis to avoid unmapped, unclassified, and non-coding genes. Volcano plots and heatmaps were created using python version 3.11.3. Enrichment heatmaps were generated using Metascape (http://metascape.org) (*60*), and enrichment networks of gene ontology (GO) pathways (GO Biological Process and GO Cellular Component) of regulated protein coding genes were visualized using the ClueGO plugin (v2.5.10) (*61*) in Cytoscape (*62*).

Statistical analysis

The statistical analyses were performed using the GraphPad Prism software, version 8.4.3. The clinical and histological data were first tested for normal distribution by the Shapiro-Wilk test. Neuronal soma sizes, due to many individual data points, were tested for normal distribution with the D'Agostino-Pearson test (Omnibus K2). Normally distributed data were tested with the F-test for homoscedasticity. Normally distributed, homoscedastic datasets were tested for significance by the unpaired, two-tailed t-test. Normally distributed datasets with unequal variance were tested for significance by the unpaired, two-tailed t-test with Welch's correction. Significance tests for non-normally distributed data were performed by the two-tailed Mann-Whitney test. The distribution underlying the Bouhassira cluster data among the groups 'neuronal loss' and 'neuronal preservation' was tested by the two-sided Fisher's exact test. Correlation analyses were performed using the Spearman test. A $p\text{-value} < 0.05$ was considered statistically significant. In boxplots, single data points are presented. The boxes extend from the 25th to the 75th percentile and the lines within the boxes show the median. The whiskers extend from the smallest to the highest value.

Abbreviations

APOJ
apolipoprotein J/clusterin
DASH
Disability arm, shoulder, and hand
DL
deep learning
DRG
dorsal root ganglia
FABP7
fatty acid binding protein 7
GFAP
glial fibrillary acidic protein
GS
glutamine synthetase
IBA1
ionized calcium-binding adapter molecule
MAP2
microtubule-associated protein 2
NF
neurofilament
NL
neuronal loss
NNA
neuron near area

NP
neuronal preservation
NPA
neuronal polygon area
NPSI
Neuropathic pain symptom inventory
NRS
numeric rating scale
ROI
regions of interest
SGC
satellite glial cells.

Declarations

Competing interests:

Authors declare that they have no competing interests. The authors declare the compliance with ethical standards including informed consent and adherence to good clinical practice.

Acknowledgements:

Funding:

Author contributions:

Conceptualization: AA, AS, JD, CM, TG, HLR, RB

Methodology: AA, AS, JD, PA, RB, HLR

Investigation: AA, AS, JD, PA, TB, RB, FS, MS, MB, GA, HLR

Software: AS

Formal analysis: AA, AS, JD, TB

Funding acquisition: JD, AS, TG, MP, HLR, RB

Supervision: CM, TG, MP, RB, HLR

Project administration: RB, HLR

Writing − original draft: AA, AS, JD, RB, HLR

Writing − review & editing: AS, RB, HLR

Data and materials availability:

Images and corresponding segmentation as well as the DL-models are available at Zenodo (*63*). The python scripts of the analysis are openly available on GitHub: https://github.com/AmSchulte/DRGhuman. RNAseq data are available through the European Genome-phenome archive, project PRJEB71432; submission ERA27745829.

References

1. P. Ciaramitaro, L. Padua, G. Devigili, E. Rota, S. Tamburin, R. Eleopra, G. Cruccu, A. Truini, S. Neuropathic pain special interest group of the Italian Neurological, Prevalence of Neuropathic Pain in Patients with Traumatic Brachial Plexus Injury: A Multicenter Prospective Hospital-Based Study. *Pain Med* **18**, 2428-2432 (2017).
2. J. A. Bertelli, M. F. Ghizoni, D. P. Loure Iro Chaves, Sensory disturbances and pain complaints after brachial plexus root injury: a prospective study involving 150 adult patients. *Microsurgery* **31**, 93-97 (2011).
3. C. Haldane, G. Frost, E. Ogalo, S. Bristol, C. Doherty, M. Berger, A systematic review and meta-analysis of patient-reported outcomes following nerve transfer surgery for brachial plexus injury. *PM R* **14**, 1368-1381 (2022).
4. N. F. Dengler, G. Antoniadis, B. Grolik, C. R. Wirtz, R. Konig, M. T. Pedro, Mechanisms, Treatment, and Patient Outcome of Iatrogenic Injury to the Brachial Plexus-A Retrospective Single-Center Study. *World Neurosurg* **107**, 868-876 (2017).
5. G. Antoniadis, H. Assmus, K. Haastert-Talini. (Springer International Publishing : Imprint: Springer,, Cham, 2017), pp. 1 online resource (VII, 143 pages 118 illustrations, 146 illustrations in color.

6. J. T. Farrar, J. P. Young, Jr., L. LaMoreaux, J. L. Werth, M. R. Poole, Clinical importance of changes in chronic pain intensity measured on an 11-point numerical pain rating scale. *Pain* **94**, 149-158 (2001).

7. J. A. Bertelli, M. F. Ghizoni, The possible role of regenerating axons in pain persistence after brachial plexus grafting. *Microsurgery* **30**, 532-536 (2010).

8. F. J. Rodríguez, A. Valero-Cabré, X. Navarro, Regeneration and functional recovery following peripheral nerve injury. *Drug Discovery Today: Disease Models* **1**, 177-185 (2004).

9. A. S. Mao, D. J. Mooney, Regenerative medicine: Current therapies and future directions. *Proc Natl Acad Sci U S A* **112**, 14452-14459 (2015).

10. M. G. Guo, D. P. Li, L. X. Wu, M. Li, B. Yang, Bone marrow mesenchymal stem cells repair brachial plexus injury in rabbits through ERK pathway. *Eur Rev Med Pharmacol Sci* **24**, 1515-1523 (2020).

11. J. Hoeber, C. Trolle, N. Konig, Z. Du, A. Gallo, E. Hermans, H. Aldskogius, P. Shortland, S. C. Zhang, R. Deumens, E. N. Kozlova, Human Embryonic Stem Cell-Derived Progenitors Assist Functional Sensory Axon Regeneration after Dorsal Root Avulsion Injury. *Sci Rep* **5**, 10666 (2015).

12. A. Schulte, H. Lohner, J. Degenbeck, D. Segebarth, H. L. Rittner, R. Blum, A. Aue, Unbiased analysis of the dorsal root ganglion after peripheral nerve injury: no neuronal loss, no gliosis, but satellite glial cell plasticity. *PAIN* **164**, 728-740 (2023).

13. X. Yu, H. Liu, K. A. Hamel, M. G. Morvan, S. Yu, J. Leff, Z. Guan, J. M. Braz, A. I. Basbaum, Dorsal root ganglion macrophages contribute to both the initiation and persistence of neuropathic pain. *Nat Commun* **11**, 264 (2020).

14. O. Avraham, P.-Y. Deng, S. Jones, R. Kuruvilla, C. F. Semenkovich, V. A. Klyachko, V. Cavalli, Satellite glial cells promote regenerative growth in sensory neurons. *Nat Commun* **11**, 4891 (2020).

15. L. T. Kuo, A. Simpson, A. Schanzer, J. Tse, S. F. An, F. Scaravilli, M. J. Groves, Effects of systemically administered NT-3 on sensory neuron loss and nestin expression following axotomy. *J Comp Neurol* **482**, 320-332 (2005).

16. M. Hanani, D. C. Spray, Emerging importance of satellite glia in nervous system function and dysfunction. *Nat Rev Neurosci* **21**, 485-498 (2020).

17. Q. Yuan, X. Liu, Y.-f. Xian, M. Yao, X. Zhang, P. Huang, W. Wu, Z.-X. Lin, Satellite glia activation in dorsal root ganglion contributes to mechanical allodynia after selective motor fiber injury in adult rats. *Biomedicine & Pharmacotherapy* **127**, 110187 (2020).

18. P. Woodham, P. N. Anderson, W. Nadim, M. Turmaine, Satellite cells surrounding axotomised rat dorsal root ganglion cells increase expression of a GFAP-like protein. *Neuroscience Letters* **98**, 8-12 (1989).

19. S. E. Jager, L. T. Pallesen, M. Richner, P. Harley, Z. Hore, S. McMahon, F. Denk, C. B. Vaegter, Changes in the transcriptional fingerprint of satellite glial cells following peripheral nerve injury. *Glia* **68**, 1375-1395 (2020).

20. A. Krishnan, S. Bhavanam, D. Zochodne, An Intimate Role for Adult Dorsal Root Ganglia Resident Cycling Cells in the Generation of Local Macrophages and Satellite Glial Cells. *Journal of Neuropathology & Experimental Neurology* **77**, 929-941 (2018).

21. H. Yu, D. Usoskin, S. S. Nagi, Y. Hu, J. Kupari, O. Bouchatta, S. L. Cranfill, M. Gautam, Y. Su, Y. Lu, J. Wymer, M. Glanz, P. Albrecht, H. Song, G.-L. Ming, S. Prouty, J. Seykora, H. Wu, M. Ma, F. L. Rice, H. Olausson, P. Ernfors, W. Luo, Single-Soma Deep RNA Sequencing of Human Dorsal Root Ganglion Neurons Reveals Novel Molecular and Cellular Mechanisms Underlying Somatosensation. *bioRxiv*, 2023.2003.2017.533207 (2023).

22. S. A. Bhuiyan, M. Xu, L. Yang, E. Semizoglou, P. Bhatia, K. I. Pantaleo, I. Tochitsky, A. Jain, B. Erdogan, S. Blair, V. Cat, J. M. Mwirigi, I. Sankaranarayanan, D. Tavares-Ferreira, U. Green, L. A. McIlvried, B. A. Copits, Z. Bertels, J. S. D. Rosario, A. J. Widman, R. A. Slivicki, J. Yi, C. J. Woolf, J. K. Lennerz, J. L. Whited, T. J. Price, R. W. G. IV, W. Renthal, Harmonized cross-species cell atlases of trigeminal and dorsal root ganglia. *bioRxiv*, 2023.2007.2004.547740 (2023).

23. M. Q. Nguyen, L. J. von Buchholtz, A. N. Reker, N. J. P. Ryba, S. Davidson, Single-nucleus transcriptomic analysis of human dorsal root ganglion neurons. *eLife* **10**, e71752 (2021).

24. O. Avraham, A. Chamessian, R. Feng, L. Yang, A. E. Halevi, A. M. Moore, R. W. t. Gereau, V. Cavalli, Profiling the molecular signature of satellite glial cells at the single cell level reveals high similarities between rodents and humans. *Pain* **163**, 2348-2364 (2022).

25. D. Tavares-Ferreira, S. Shiers, P. R. Ray, A. Wangzhou, V. Jeevakumar, I. Sankaranarayanan, A. M. Cervantes, J. C. Reese, A. Chamessian, B. A. Copits, P. M. Dougherty, R. W. t. Gereau, M. D. Burton, G. Dussor, T. J. Price, Spatial transcriptomics of dorsal root ganglia identifies molecular signatures of human nociceptors. *Sci Transl Med* **14**, eabj8186 (2022).

26. S. Shiers, R. M. Klein, T. J. Price, Quantitative differences in neuronal subpopulations between mouse and human dorsal root ganglia demonstrated with RNAscope in situ hybridization. *PAIN* **161**, 2410-2424 (2020).

27. B. E. Hall, E. Macdonald, M. Cassidy, S. Yun, M. R. Sapio, P. Ray, M. Doty, P. Nara, M. D. Burton, S. Shiers, A. Ray-Chaudhury, A. J. Mannes, T. J. Price, M. J. Iadarola, A. B. Kulkarni, Transcriptomic analysis of human sensory neurons in painful diabetic neuropathy reveals inflammation and neuronal loss. *Scientific reports* **12**, 4729 (2022).

28. P. R. Ray, S. Shiers, J. P. Caruso, D. Tavares-Ferreira, I. Sankaranarayanan, M. L. Uhelski, Y. Li, R. Y. North, C. Tatsui, G. Dussor, M. D. Burton, P. M. Dougherty, T. J. Price, RNA profiling of human dorsal root ganglia reveals sex-differences in mechanisms promoting neuropathic pain. *Brain* **146**, 749−766 (2022).

29. D. Segebarth, M. Griebel, N. Stein, C. R. von Collenberg, C. Martin, D. Fiedler, L. B. Comeras, A. Sah, V. Schoeffler, T. Lüffe, A. Dürr, R. Gupta, M. Sasi, C. Lillesaar, M. D. Lange, R. O. Tasan, N. Singewald, H.-C. Pape, C. M. Flath, R. Blum, On the objectivity, reliability, and validity of deep learning enabled bioimage analyses. *eLife* **9**, e59780 (2020).

30. D. Bouhassira, S. Branders, N. Attal, A. M. Fernandes, D. Demolle, J. Barbour, D. Ciampi de Andrade, A. Pereira, Stratification of patients based on the Neuropathic Pain Symptom Inventory: development and validation of a new algorithm. *Pain* **162**, 1038-1046 (2021).

31. D. M. Pelt, Tackling the challenges of bioimage analysis. *Elife* **9**, e64384 (2020).

32. D. Usoskin, A. Furlan, S. Islam, H. Abdo, P. Lonnerberg, D. Lou, J. Hjerling-Leffler, J. Haeggstrom, O. Kharchenko, P. V. Kharchenko, S. Linnarsson, P. Ernfors, Unbiased classification of sensory neuron types by large-scale single-cell RNA sequencing. *Nat Neurosci* **18**, 145-153 (2015).

33. J. Kupari, P. Ernfors, Molecular taxonomy of nociceptors and pruriceptors. *PAIN* **164**, 1245-1257 (2023).

34. M. Socolovsky, G. Antoniadis, A. Lovaglio, G. Durner, G. Bonilla, M. Schmidhammer, G. di Masi, A Comparison of Patients from Argentina and Germany to Assess Factors Impacting Brachial Plexus and Brain Injury. *J Brachial Plex Peripher Nerve Inj* **14**, e39-e46 (2019).

35. W. Faglioni, Jr., M. G. Siqueira, R. S. Martins, C. O. Heise, L. Foroni, The epidemiology of adult traumatic brachial plexus lesions in a large metropolis. *Acta Neurochir (Wien)* **156**, 1025-1028 (2014).

36. R. Midha, Epidemiology of brachial plexus injuries in a multitrauma population. *Neurosurgery* **40**, 1182-1188; discussion 1188-1189 (1997).

37. H. Suroto, R. A. Putra, A. Karimah, Relationship between disability and pain to post-traumatic stress disorder, depression, and anxiety in patient with postoperative brachial plexus injury (BPI). *Br J Neurosurg* **35**, 254-258 (2021).

38. C. Roza, L. Bernal, Electrophysiological characterization of ectopic spontaneous discharge in axotomized and intact fibers upon nerve transection: a role in spontaneous pain? *Pflugers Arch* **474**, 387-396 (2022).

39. S. Haroutounian, L. Nikolajsen, T. F. Bendtsen, N. B. Finnerup, A. D. Kristensen, J. B. Hasselstrom, T. S. Jensen, Primary afferent input critical for maintaining spontaneous pain in peripheral neuropathy. *Pain* **155**, 1272-1279 (2014).

40. N. B. Finnerup, N. Attal, S. Haroutounian, E. McNicol, R. Baron, R. H. Dworkin, I. Gilron, M. Haanpää, P. Hansson, T. S. Jensen, P. R. Kamerman, K. Lund, A. Moore, S. N. Raja, A. S. Rice, M. Rowbotham, E. Sena, P. Siddall, B. H. Smith, M. Wallace, Pharmacotherapy for neuropathic pain in adults: a systematic review and meta-analysis. *Lancet Neurol* **14**, 162-173 (2015).

41. P. Anand, R. Birch, Restoration of sensory function and lack of long-term chronic pain syndromes after brachial plexus injury in human neonates. *Brain* **125**, 113-122 (2002).

42. H. Aldskogius, E. N. Kozlova, Dorsal Root Injury-A Model for Exploring Pathophysiology and Therapeutic Strategies in Spinal Cord Injury. *Cells* **10**, 2185 (2021).

43. D. J. Chew, K. Murrell, T. Carlstedt, P. J. Shortland, Segmental spinal root avulsion in the adult rat: a model to study avulsion injury pain. *J Neurotrauma* **30**, 160-172 (2013).

44. R. E. Zigmond, F. D. Echevarria, Macrophage biology in the peripheral nervous system after injury. *Prog Neurobiol* **173**, 102-121 (2019).

45. M. Griebel, D. Segebarth, N. Stein, N. Schukraft, P. Tovote, R. Blum, C. M. Flath, Deep learning-enabled segmentation of ambiguous bioimages with deepflash2. *Nature communications* **14**, 1679 (2023).

46. S. Weiner, M. Strinitz, J. Herfurth, F. Hessenauer, C. Nauroth-Kress, T. Kampf, G. A. Homola, N. Uceyler, C. Sommer, M. Pham, M. Schindehutte, Dorsal Root Ganglion Volumetry by MR Gangliography. *AJNR*

Am J Neuroradiol **43**, 769-775 (2022).

47. C. Dietz, M. Muller, A. K. Reinhold, L. Karch, B. Schwab, L. Forer, E. Vlckova, E. M. Brede, R. Jakubietz, N. Uceyler, R. Meffert, J. Bednarik, M. Kress, C. Sommer, V. Dimova, F. Birklein, H. L. Rittner, What is normal trauma healing and what is complex regional pain syndrome I? An analysis of clinical and experimental biomarkers. *Pain* **160**, 2278-2289 (2019).

48. M. Von Korff, J. Ormel, F. J. Keefe, S. F. Dworkin, Grading the severity of chronic pain. *Pain* **50**, 133-149 (1992).

49. P. L. Hudak, P. C. Amadio, C. Bombardier, Development of an upper extremity outcome measure: the DASH (disabilities of the arm, shoulder and hand) [corrected]. The Upper Extremity Collaborative Group (UECG). *Am J Ind Med* **29**, 602-608 (1996).

50. C. Kühner, C. Bürger, F. Keller, M. Hautzinger, Reliabilität und Validität des revidierten Beck-Depressionsinventars (BDI-II). *Der Nervenarzt* **78**, 651-656 (2007).

51. L. J. Julian, Measures of anxiety: State-Trait Anxiety Inventory (STAI), Beck Anxiety Inventory (BAI), and Hospital Anxiety and Depression Scale-Anxiety (HADS-A). *Arthritis Care Res (Hoboken)* **63 Suppl 11**, S467-472 (2011).

52. M. J. Sullivan, S. R. Bishop, J. Pivik, Pain Catastrophizing scale. *The Journal of Pain*, (2009).

53. T. Kretschmer, S. Ihle, G. Antoniadis, J. A. Seidel, C. Heinen, W. Börm, H. P. Richter, R. König, Patient satisfaction and disability after brachial plexus surgery. *Neurosurgery* **65**, A189-196 (2009).

54. P. Bankhead, M. B. Loughrey, J. A. Fernández, Y. Dombrowski, D. G. McArt, P. D. Dunne, S. McQuaid, R. T. Gray, L. J. Murray, H. G. Coleman, J. A. James, M. Salto-Tellez, P. W. Hamilton, QuPath: Open source software for digital pathology image analysis. *Scientific reports* **7**, 16878 (2017).

55. T. Smith, A. Heger, I. Sudbery, UMI-tools: modeling sequencing errors in Unique Molecular Identifiers to improve quantification accuracy. *Genome Res* **27**, 491-499 (2017).

56. M. Martin, Cutadapt removes adapter sequences from high-throughput sequencing reads. *EMBnet J.* **17**, 10 (2011).

57. A. Dobin, C. A. Davis, F. Schlesinger, J. Drenkow, C. Zaleski, S. Jha, P. Batut, M. Chaisson, T. R. Gingeras, STAR: ultrafast universal RNA-seq aligner. *Bioinformatics* **29**, 15-21 (2013).

58. Y. Liao, G. K. Smyth, W. Shi, featureCounts: an efficient general purpose program for assigning sequence reads to genomic features. *Bioinformatics* **30**, 923-930 (2014).

59. M. I. Love, W. Huber, S. Anders, Moderated estimation of fold change and dispersion for RNA-seq data with DESeq2. *Genome Biology* **15**, 550 (2014).

60. Y. Zhou, B. Zhou, L. Pache, M. Chang, A. H. Khodabakhshi, O. Tanaseichuk, C. Benner, S. K. Chanda, Metascape provides a biologist-oriented resource for the analysis of systems-level datasets. *Nat Commun* **10**, 1523 (2019).

61. G. Bindea, B. Mlecnik, H. Hackl, P. Charoentong, M. Tosolini, A. Kirilovsky, W. H. Fridman, F. Pagès, Z. Trajanoski, J. Galon, ClueGO: a Cytoscape plug-in to decipher functionally grouped gene ontology and pathway annotation networks. *Bioinformatics* **25**, 1091-1093 (2009).

62. P. Shannon, A. Markiel, O. Ozier, N. S. Baliga, J. T. Wang, D. Ramage, N. Amin, B. Schwikowski, T. Ideker, Cytoscape: a software environment for integrated models of biomolecular interaction networks. *Genome Res* **13**, 2498-2504 (2003).

63. A. Sodmann, J. Degenbeck, A. Aue, M. Schindehütte, F. Schlott, P. Arampatzi, T. Bischler, M. Schneider, C. M. Monoranu, T. Gräfenhan, M. Bohnert, M. Pham, G. Antoniadis, R. Blum, H. L. Rittner, Data from: Molecular and cellular processes of deafferentation after plexus injury in human dorsal root ganglia. *Zenodo*, (2022).

Supplementary Materials

Data files S1 and S2 are not available with this version.

Figures
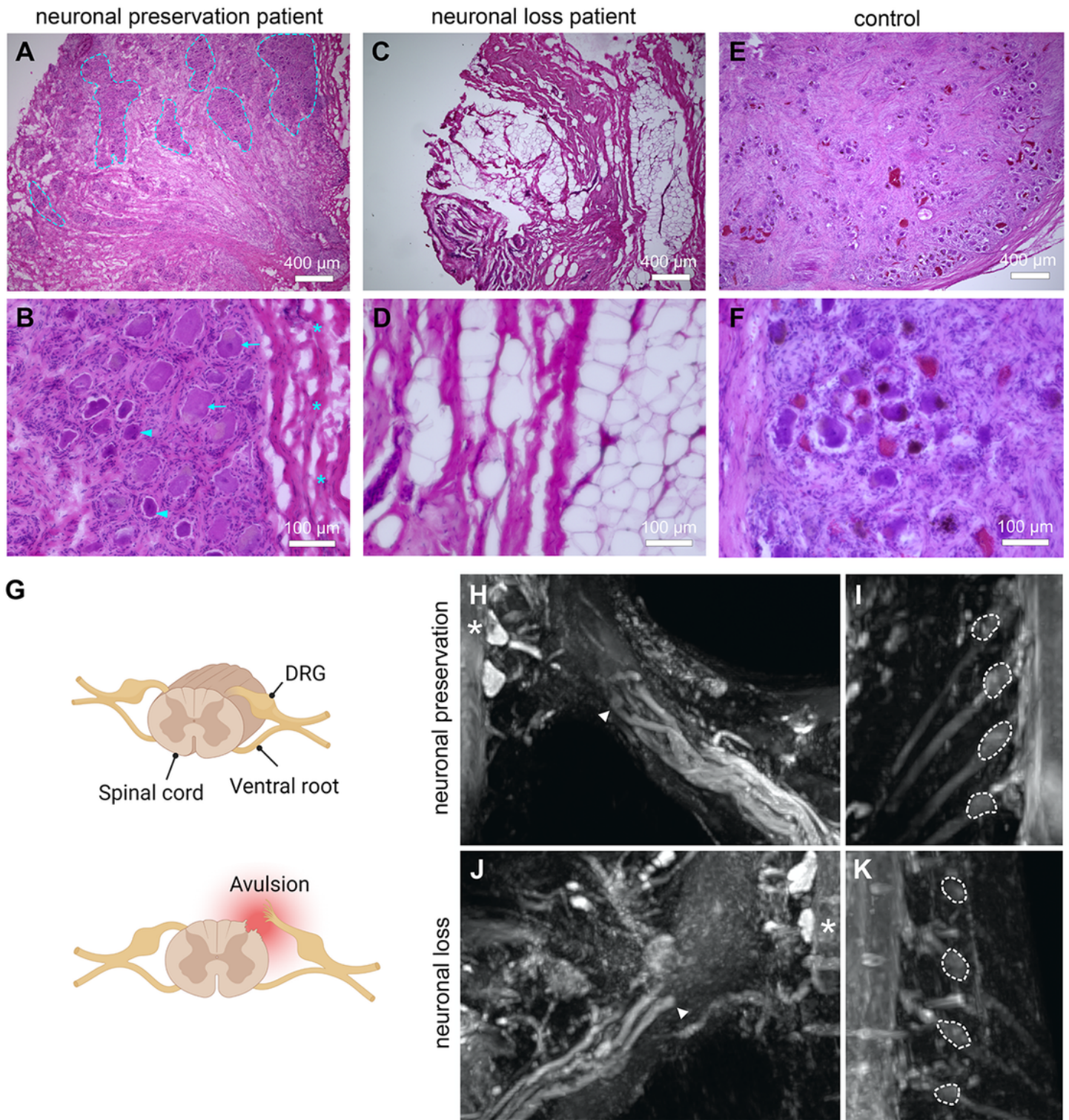
Figure 1

Classification into 'neuronal preservation' or 'neuronal loss'. (A-F) Representative images of H&E-stained sections of DRG from plexus injury patients. Indicated are: neuron-rich area (outlined in A), small sensory neurons (arrowheads in B), large sensory neurons (arrows in B), connective tissue (asterisks in B). (G) Scheme of DRG depicting a dorsal root avulsion (image created with biorender). (H-K) Images resulting from magnetic resonance neurography of the brachial plexus in dorsal root avulsion patients, each

representing one patient group. In both groups affected DRG can no longer be identified, nor their volume quantified. Indicated are nerve stumps (arrowheads in H and J) and pseudomeningoceles of C8 roots (asterisks in H and J) as well as unaffected DRG at C5-C8 of the corresponding contralateral side (dotted line in I and K).
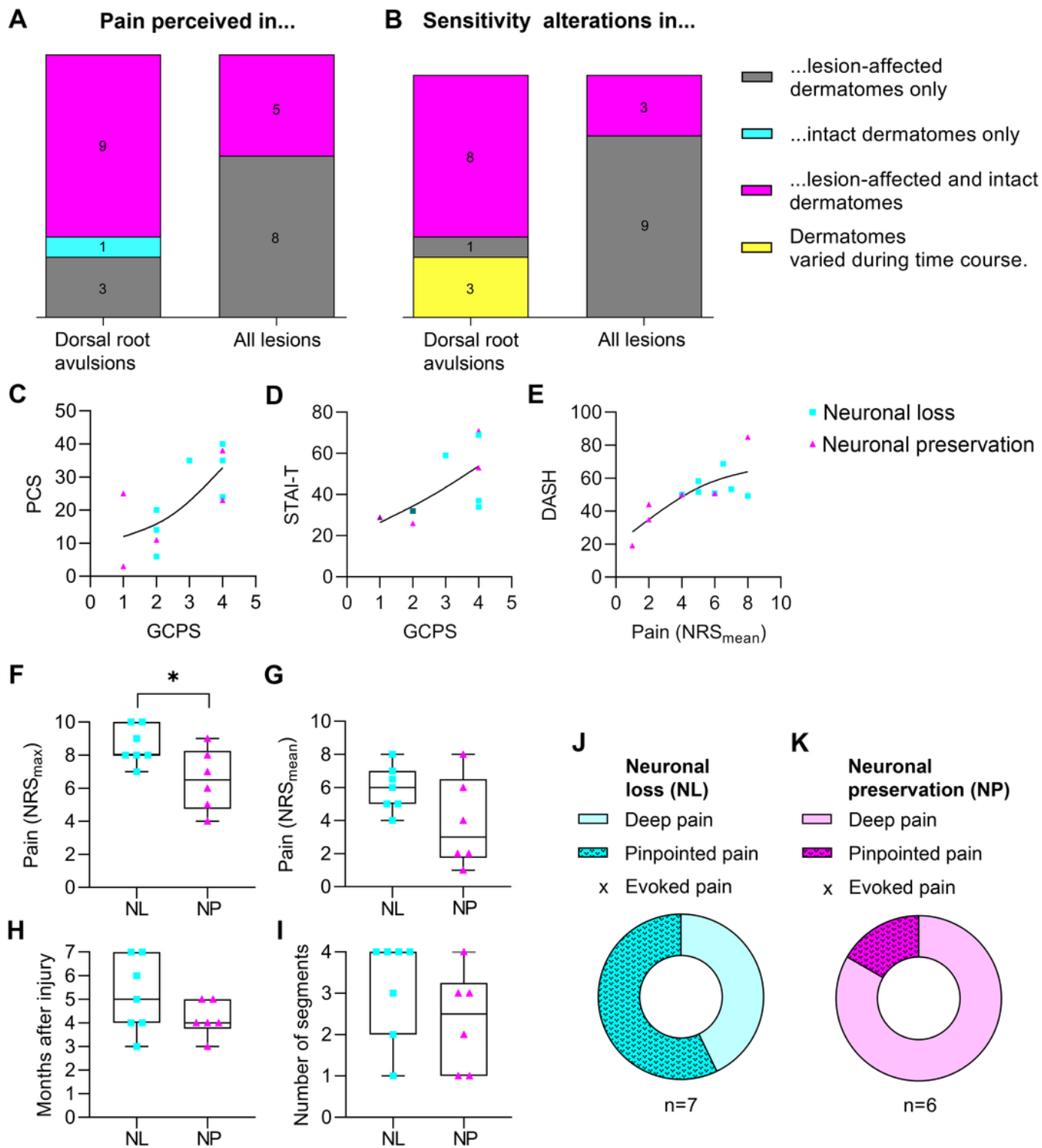

Figure 2

Clinical symptoms and disease severity in patients with DRG preservation and DRG loss. (**A**) Areas of reported pain matched to dermatomes. (**B**) Areas of sensitivity alterations, e. g. allodynia or dysesthesia, or numbness, matched to dermatomes. Sensitivity alteration data of one patient was not available. Patients were assigned to four categories. *In grey:* Patients with symptoms only in dermatomes supplied by corresponding avulsed dorsal roots. *In cyan:* Patients with symptoms in dermatomes supplied by intact roots. *In magenta:* Patients with symptoms in dermatomes supplied by intact and avulsed roots. *In yellow:* Patients who reported different sensitivity changes after the accident and before surgery. Left columns: Dermatomes normally supplied by avulsed dorsal roots. Right columns: Dermatomes potentially affected by any kind of lesion. (**C-E**) Correlation of pain with psychiatric comorbidities in patients after plexus injury. (**C**) Pain Catastrophizing Scale (PCS) in relation to the von Korff's Graded Chronic Pain Scale (GCPS, Spearman test, r = 0.6751, p = 0.0197). (**D**) Trait-anxiety reported in the State-Trait-Anxiety Inventory (STAI-T) compared with the GCPS (Spearman test, r = 0.8405, p = 0.0013). Single patient data: dark magenta marks two 'neuronal preservation' patients; dark cyan marks three 'neuronal loss' patients. (**E**) Disability of the Arm, Shoulder, and Hand score (DASH disability/ symptom score) in comparison to mean pain on the Numeric Rating Scale (NRS) during the last four weeks before surgery (Spearman test, r = 0.6981, p = 0.0098). Patients with 'neuronal loss' are depicted in cyan, the 'neuronal preservation' group is shown in magenta. Trends are shown as black line (**F-K**) Comparison of clinical data of patients with 'neuronal preservation' or 'neuronal loss'. (**F**) Maximal pain on the numeric rating scale (NRS) during the last four weeks before surgery (unpaired, two-tailed t-test, *p = 0.0317). (**G**) Mean pain according to NRS (unpaired, two-tailed t-test, p = 0.0990, not significant). (**H**) Time between injury and reconstructive surgery in months (unpaired, two-tailed t-test, p = 0.1939, not significant). (**I**) Number of dorsal roots affected by dorsal root avulsion (two-tailed Mann-Whitney test, p = 0.2541, not significant). (**J, K**) Neuropathic pain phenotype according to Bouhassira clusters. No patient reported evoked pain. Two-sided Fisher's exact test, p = 0.2657, not significant. Number of patients: 'neuronal loss' group: n = 7; 'neuronal preservation' group: n = 6.
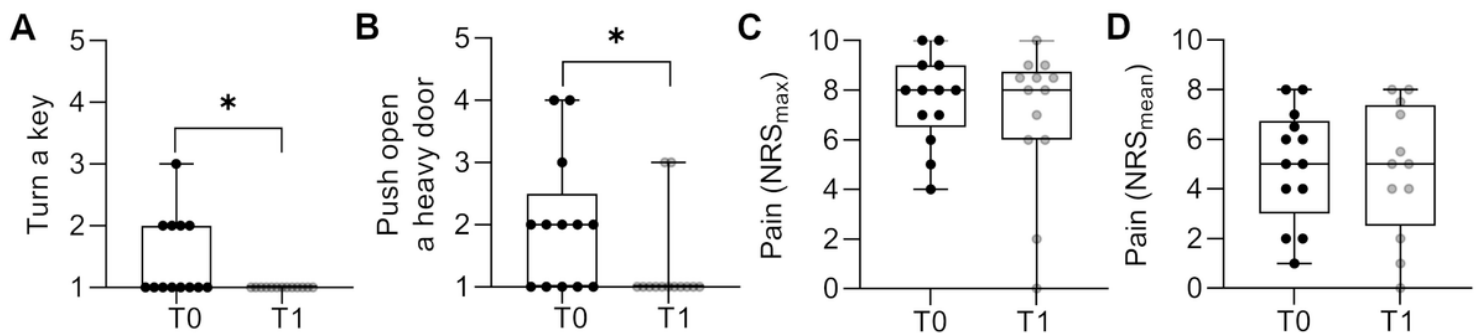

Figure 3

Functional recovery but persistence of pain. (**A-B**) Functional improvements at the time point of the telephone interview (T1) compared to the time point of surgery (T0). Disability of arm, shoulder, and hand (DASH): symptom score, item 3: Ability to turn a key, scaled from 1-5 (two-tailed Mann-Whitney test, *p = 0.0391, in A). Ability to push open a heavy door (two-tailed Mann-Whitney test, *p=0.0355, in B). (**C-D**)

Pain intensity at the time point of surgery (T0) compared to the time point of the telephone interview (T1). Maximum pain (two-tailed Mann-Whitney-Test, p = 0.909, not significant, in C). Mean pain (unpaired, two tailed t-test, p = 0.8334, not significant, in D).
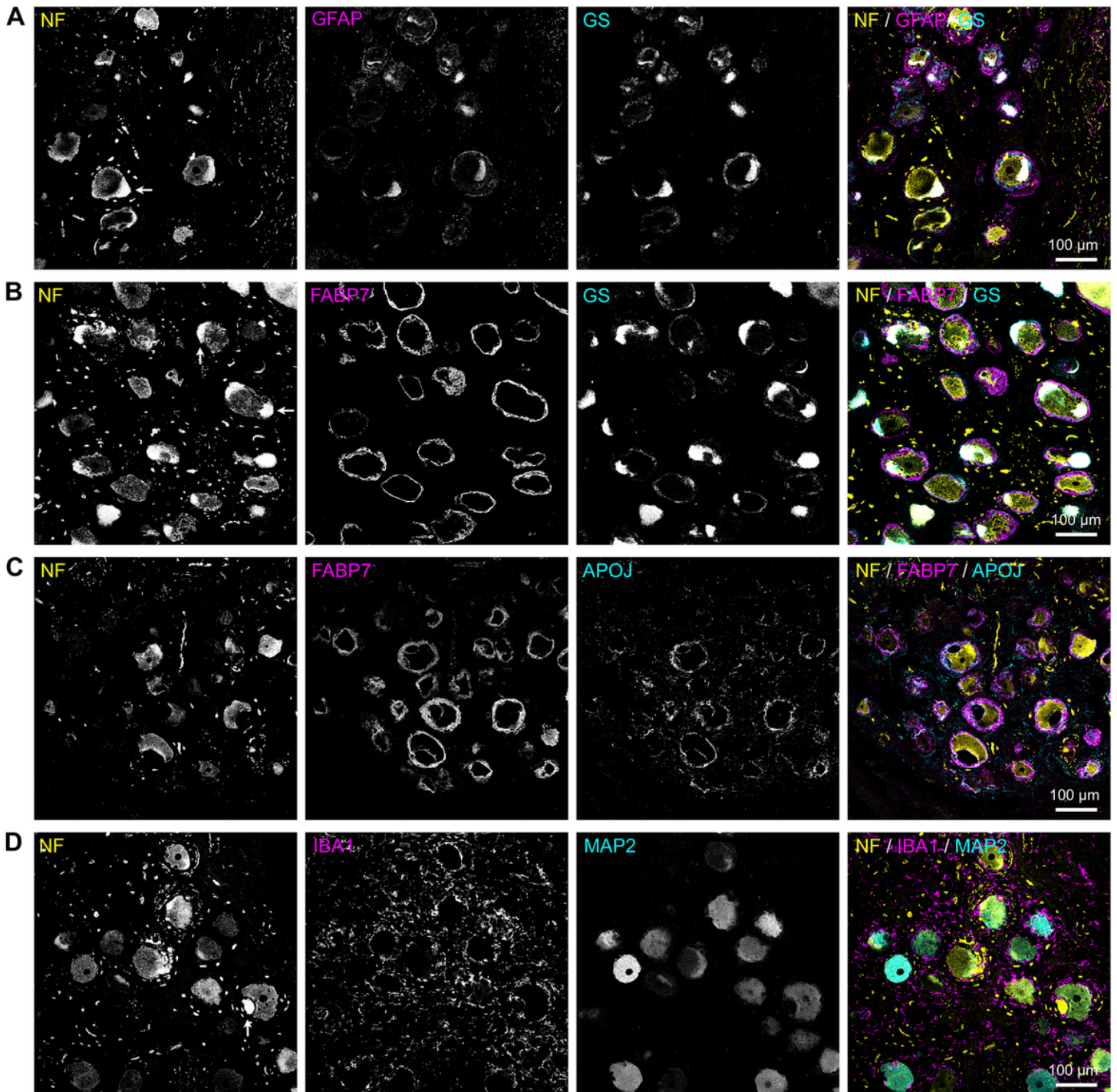

Figure 4

Immunofluorescence labeling of human DRG. (A-D) Representative confocal images (maximum intensity projection) show DRG labels from plexus injury patients. Neurons were labeled with indicated markers. NF (neurofilament, yellow, in A-D) and MAP2 (microtubule-associated protein 2, cyan, in D). Satellite glial

cells were marked using GFAP (glial fibrillary acidic protein, magenta, in A), GS (glutamine synthetase, cyan, in A), FABP7 (fatty acid binding protein 7, magenta, in B, C) and APOJ (clusterin, cyan, in C). Macrophages were labeled with IBA1 (ionized calcium binding adaptor molecule 1, in D). Lipofuscin-mediated autofluorescence was observed in all tissue samples (see arrows). Scale bar: 100 µm.
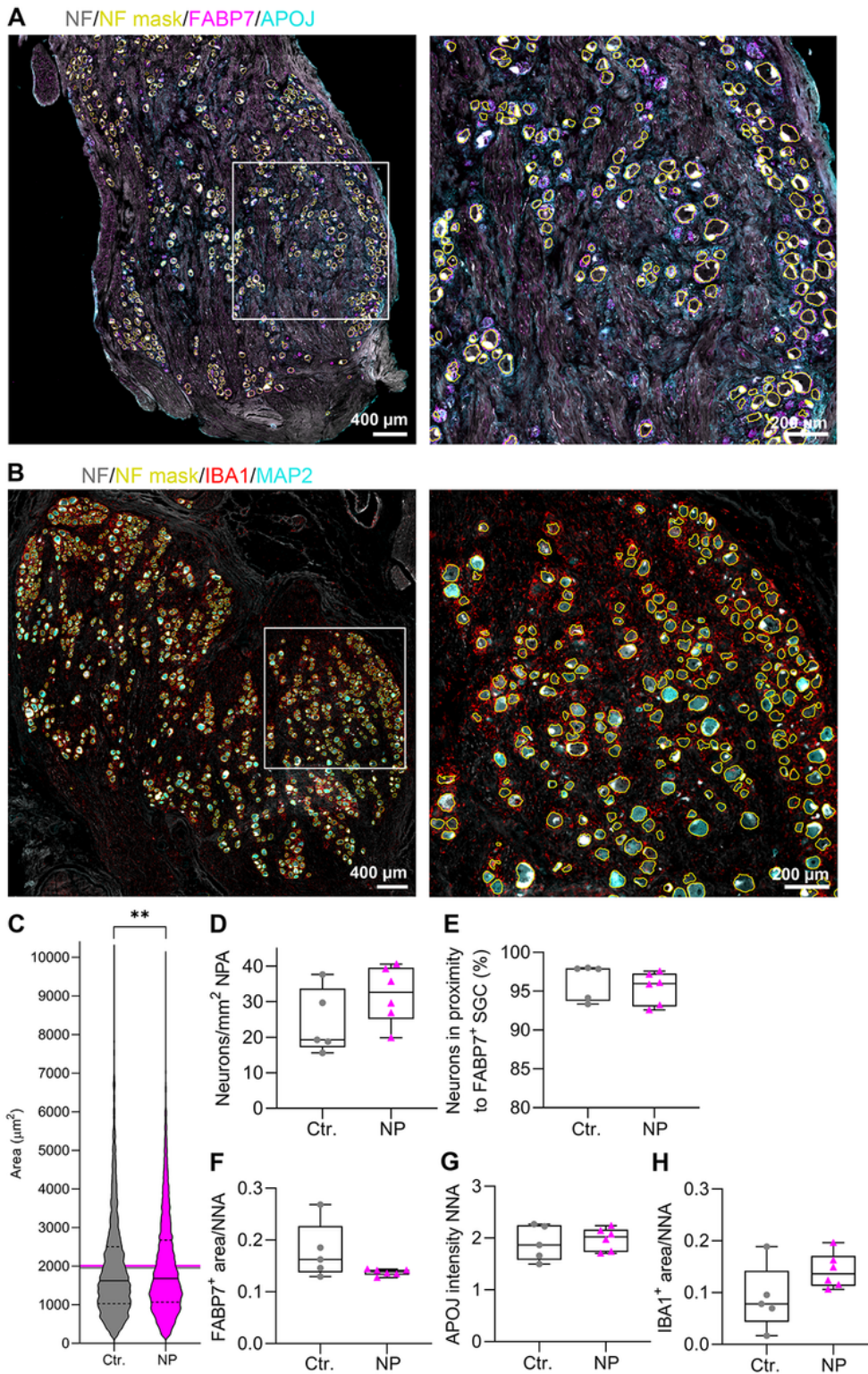

Figure 5

Cellular composition of DRG from patients with 'neuronal preservation' vs. control. Immunohistochemical analysis comparing control (Ctr., grey, circles, n = 5) versus 'neuronal preservation' DRG (NP, magenta, triangles, n = 6). (**A**) Representative images of a patient DRG section with neurons (NF, grey) and SGC (FABP7, magenta; APOJ cyan). NF-positive neurons were segmented with a deep learning model (NF mask, yellow). (**B**) Labelling of neurons (NF, grey; NF-mask, yellow; MAP2, cyan) and macrophages (IBA1, red). (**C**) Violin plot showing the soma size of neurons. Black lines: median area of neuronal somata, dashed lines: 25th and 75th percentile, lines in grey and magenta: mean area of control and 'neuronal preservation' DRG (two-tailed Mann-Whitney test, **p = 0.0050). (**D**) Number of neurons per mm^2 in the neuron-rich area (computed as neuronal polygon area, NPA) (unpaired, two-tailed t-test, p = 0.1689, not significant). (**E**) Percentage of neurons in proximity to FABP7-positive satellite glial cells (SGC, two-tailed Mann-Whitney test, p = 0.2468, not significant). (**F**) Neuron near area (NNA) in close proximity to FABP7-positive cells (unpaired, two-tailed t-test with Welch's correction, p = 0.1698, not significant). (**G**) Intensity of the anti-APOJ signal in SGC normalized to the intensity of the APOJ signal in the neuron near area (NNA, unpaired, two-tailed t-test, p = 0.6681, not significant). (**H**) Neuron near area (NNA) occupied by IBA1 positive macrophages (unpaired, two-tailed t-test, p = 0.1111, not significant).
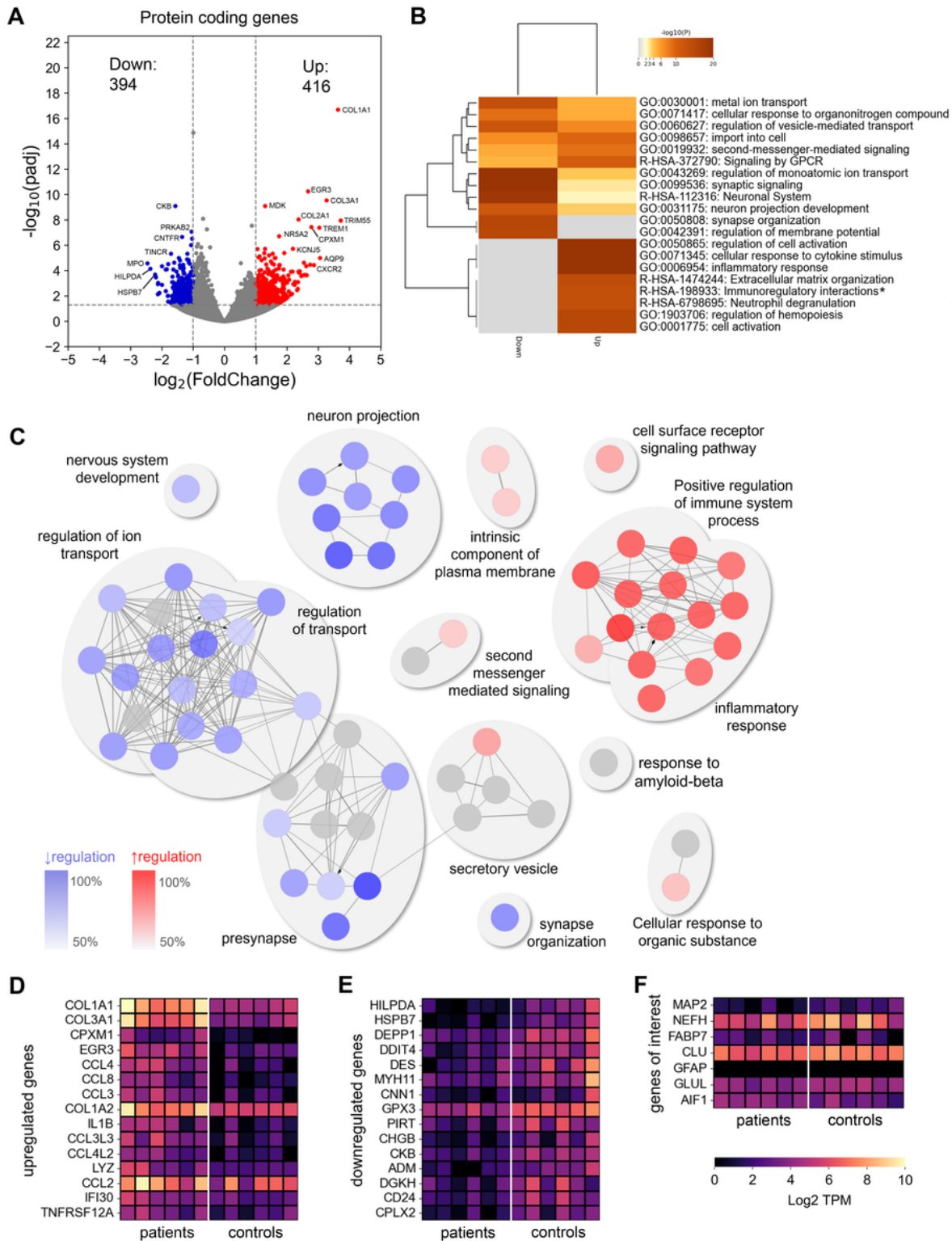
Figure 6

Transcriptional changes in DRG from patients with 'neuronal preservation' vs. control. (A) Volcano plot of significantly upregulated (red) and downregulated (blue) protein coding genes (padj < 0.05 and -1 > log2FC > 1). **(B)** Top terms of significantly up- and downregulated genes, colored by p-values using Metascape. *Immunoregulatory interactions between a Lymphoid and a non-Lymphoid cell. **(C)** Gene ontology (GO) pathway (GO Biological Process and GO Cellular Component) analysis of regulated protein

coding genes in ClueGO (v2.5.10). Only pathways with p-values < $1*10^{-6}$ (Bonferroni step down corrected) are shown. Top term-term interactions of regulated protein coding genes appear in corresponding clusters. Each node represents a GO term. Colors indicate upregulated components in red; downregulated in blue. Grey nodes harbor proteins from both regulatory lists and cannot be unambiguously assigned. Cluster terms are based on the highest significance. (**D**) Heatmap of transcriptomic expression of top 15 significantly upregulated and (**E**) downregulated genes. Shown are transcripts per million (TPM) values, filtered according to >10 TPM in either patient or control group, sorted by Log2FC. (**F**) Transcriptome data of the genes whose proteins were stained by immunofluorescence (Fig. 3). Scale bar: Log2 TPM.
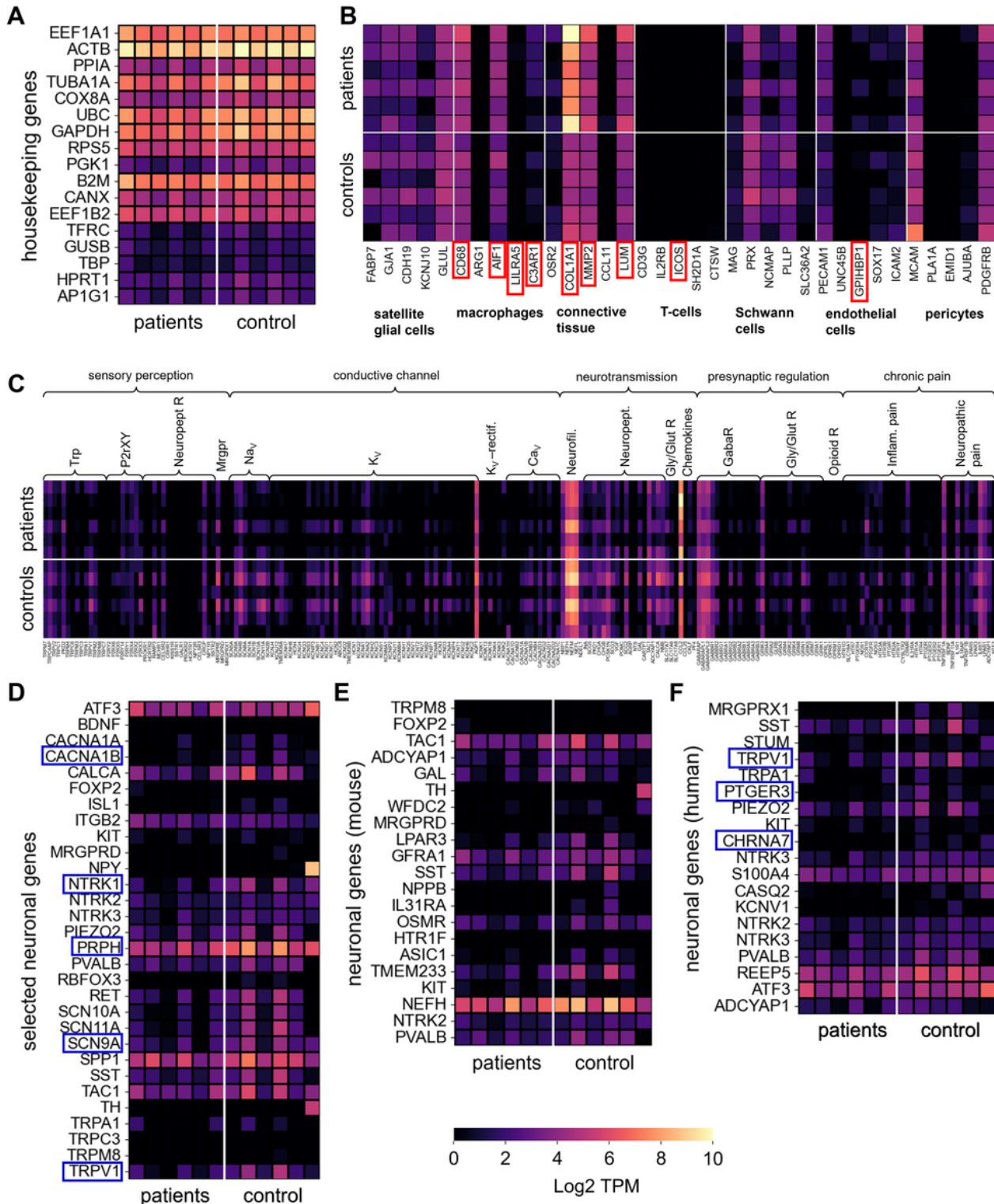
Figure 7

Upregulation of macrophage and connective tissue markers, but downregulation of neuronal markers. Heatmaps of transcriptomic expression of **(A)** housekeeping genes, **(B)** marker genes of non-neuronal cells in the DRG (*14, 19*), **(C)** different operational components of sensory neurons (*32*), **(D)** selected neuronal genes, **(E)** and marker genes of different neuronal subtypes found in mice (*33*) and **(F)**

humans (*21*). Marked are significantly upregulated (red) and downregulated (blue) genes (padj < 0.05 and -1 > log2FC > 1), for C see Data File S2. Scale bar: Log2 TPM.

Supplementary Files

This is a list of supplementary files associated with this preprint. Click to download.

- SupplementalMaterialSodmannPlexusPaper.docx